



CHORUS

This is the accepted manuscript made available via CHORUS. The article has been published as:

Slicing dependence of nonspherically symmetric quasilocal horizons in Vaidya spacetimes

Alex B. Nielsen, Michael Jasiulek, Badri Krishnan, and Erik Schnetter

Phys. Rev. D **83**, 124022 — Published 10 June 2011

DOI: [10.1103/PhysRevD.83.124022](https://doi.org/10.1103/PhysRevD.83.124022)

The slicing dependence of non-spherically symmetric quasi-local horizons in Vaidya spacetimes

Alex B. Nielsen,^{1,*} Michael Jasiulek,^{1,†} Badri Krishnan,^{1,‡} and Erik Schnetter^{2,3,§}

¹*Max-Planck-Institut für Gravitationsphysik, Albert-Einstein-Institut, Am Mühlenberg 1, D-14476 Golm, Germany*

²*Center for Computation & Technology, 216 Johnston Hall, Louisiana State University, Baton Rouge, LA 70803, USA*

³*Department of Physics & Astronomy, 202 Nicholson Hall, Louisiana State University, Baton Rouge, LA 70803, USA*

It is well known that quasi-local black hole horizons depend on the choice of a time coordinate in a spacetime. This has implications for notions such as the surface of the black hole and also on quasi-local physical quantities such as horizon measures of mass and angular momentum. In this paper, we compare different horizons on non-spherically symmetric slicings of Vaidya spacetimes. The spacetimes we investigate include both accreting and evaporating black holes. For some simple choices of the Vaidya mass function corresponding to collapse of a hollow shell, we compare the area for the numerically found axisymmetric trapping horizons with the area of the spherically symmetric trapping horizon and event horizon. We find that as expected, both the location and area are dependent on the choice of foliation. However, the area variation is not large, of order 0.017% for a slowly evolving horizon with $\dot{m} = 0.02$. We also calculate analytically the difference in area between the spherically symmetric quasi-local horizon and event horizon for a slowly accreting black hole. We find that the difference can be many orders of magnitude larger than the Planck area for sufficiently large black holes.

PACS numbers: 04.25.dg, 04.70.-s, 04.70.Bw

I. INTRODUCTION

An important feature of black hole spacetimes is the existence of trapped and marginally trapped surfaces. These surfaces are a key element in the Penrose singularity theorem and are frequently used in numerical relativity to indicate the existence of a black hole. Recent work has introduced related concepts such as trapping horizons and dynamical horizons both of which, ignoring certain technical conditions, can be viewed 3-surfaces obtained by time-evolutions of marginally trapped surfaces; these are thus 3-surfaces foliated by marginally trapped surfaces. It has been shown that these surfaces have many properties similar to event horizons, in particular their thermodynamic properties [1–3]. Trapping and dynamical horizons can also be used to extract data about the black hole, such as its mass and angular momentum, directly from the strong gravity region without needing to rely on the asymptotic behaviour or exact isometries [1].

However, it has been known for a long time that the location and existence of trapped surfaces depends on the choice of spacetime foliation, i.e. on the choice of the time coordinate, and this is the main reason why event horizons have often been preferred over trapping and dynamical horizons as a definition of the surface of a black hole. In particular this means that any given, suitably general, spacetime that contains a trapping horizon is likely to contain, in principle, an infinite number of trapping and dynamical horizons [4]. The key results for quasi-local

horizons, for example the laws of black hole mechanics and the energy and angular momentum balance laws [5], are sufficiently general and are applicable to all of these different horizons. Nevertheless, if we wish to assign say mass and spin to the black hole quasi-locally, the time evolution of these quantities will depend on which horizon we choose to use. Thus, to use quasi-local horizons to extract meaningful data from black hole spacetimes it is important to investigate the location of these distinct horizons and how this affects their related properties such as mass, angular momentum, linear momentum etc.

This issue is potentially relevant for gravitational wave astronomy when one seeks to infer the physical parameters of the source from the observed gravitational wave signal. For example, in modeling binary black hole coalescence it becomes important to combine results from post-Newtonian theory and numerical relativity. Numerical relativity can in principle evolve a binary black hole system starting from the inspiral phase all the way through the coalescence (see e.g. [6] for a recent review). However, this becomes computationally impossible if we start the black holes very far apart, and if we wish to cover a large parameter space. Post-Newtonian theory on the other hand treats the black holes as point particles endowed with a mass and spin, and solves the field equations in powers of v/c with v being the orbital velocity of the black holes. This approximation works best when the black holes are far apart and breaks down near the coalescence. Thus, in order to fully solve the binary black hole problem it becomes essential to combine the two frameworks. The literature on this topic is large and a full discussion is beyond the scope of this paper; see e.g. [7–13]. For our purposes, we note that the two frameworks treat black holes very differently; post-Newtonian theory treats the black holes as point particles while numerical

* alex.nielsen@aei.mpg.de

† michael.jasiulek@aei.mpg.de

‡ badri.krishnan@aei.mpg.de

§ schnetter@cct.lsu.edu

relativity deals with the horizons non-perturbatively. It turns out that using different flavors of Post-Newtonian approximants leads to biases in the values of physical parameters [14] (as inferred from the gravitational waveforms). Numerical relativity on the other hand deals with black hole horizons, and if we decide to use quasi-local horizon measures for calculating physical quantities, the values of the black hole parameters will be affected by the choice of foliation. This effect is absent when the black holes are isolated; thus we expect it to be negligible in the inspiral phase and to be larger in the dynamical coalescence phase. In comparing the results from the two frameworks, it is useful then to quantify this source of uncertainty and to show that errors in the physical parameters are smaller than the biases between, say, different post-Newtonian approximants.

Another area where the location of horizons is important is in black hole thermodynamics. If the area of a black hole horizon is to play a role analogous to entropy via the Bekenstein-Hawking relation it is important to know which area this relation should be applied to in which situations. For stationary black holes, cross-sections of the event horizon are marginally trapped surfaces and thus the different notions of black hole horizons (i.e. event horizons and trapping horizons) coincide. However, in a dynamical spacetime the event horizon will not coincide with the location of any of the trapping horizons. In general they will have different areas on a given spacelike hypersurface [15, 16]. Furthermore, although the location of the event horizon does not depend on the choice of spacetime foliation, when the event horizon is growing or shrinking, its area will depend on the choice of foliation.

Non-stationary spacetimes with dynamical black holes are complicated, and only a few exact dynamical black hole solutions are known. One class of solutions is the Vaidya solutions, which describe the evolution of a spherically symmetric, radially moving, pressureless null fluid with a freely specifiable mass function $m(v)$. This is a useful and non-trivial toy-model for a dynamical black hole. These spacetimes can be used to qualitatively model the physical accretion of matter by a black hole. Some authors [17, 18] have even suggested using the Vaidya spacetimes to simulate the decrease in area of a black hole due to Hawking radiation, by allowing the infalling matter to have negative energy.

While there is a unique event horizon in a black hole spacetime, this is not true for dynamical horizons. As mentioned above, a black hole spacetime may contain infinitely many dynamical/trapping horizons and thus far there is no generally satisfactory method of picking a preferred one. The non-uniqueness of dynamical horizons in general spacetimes was investigated in [4]. Two results proved in [4] which are important for our purposes are: (i) The foliation of a given dynamical horizon by marginally trapped surfaces is unique. (ii) While there are numerous dynamical horizons in the black hole region of a spacetime, they are not so numerous as to form a foliation of

any spacetime region. Thus, two dynamical horizons are either well separated and lie in distinct spacetime regions, or they are mutually intersecting. We will show explicit examples and study the properties of such mutually intersecting dynamical horizons in the Vaidya spacetime.

In the Vaidya solution it has already been shown explicitly that marginally outer trapped surfaces (MOTS) can be found at various different locations depending on the slicing [19], although this reference did not investigate how the parameters of the black hole, such as area, mass and angular momentum vary with slicing and did not consider the case of timelike trapping horizons. Ben-Dov [20] showed how to find marginally outer trapped surfaces arbitrarily close to the event horizon. It was also shown that there are flat regions inside the event horizon (the region contained within the shell) where no trapped surface passes. Bengtsson and Senovilla [21] analytically constructed trapped surfaces that pass through the flat region. This is not a contradiction; while there are some flat regions where no trapped surface can be located, there are trapped surfaces in other parts of the flat region. In spherically symmetric spacetimes spherically symmetric marginally trapped surfaces are easy to find and in the case of Vaidya are given by the condition $r = 2m(v)$, where r is the areal coordinate ($r = \sqrt{A/16\pi}$ with A being the area of the MOTS) of the surfaces of spherical isometry. It is also easy to show that such surfaces foliate a trapping horizon which we will refer to as the spherically symmetric trapping horizon. Due to results in [4], any other dynamical horizon will lie partially outside the spherically symmetric dynamical horizon somewhere. For example, in [22] analytic solutions were presented where closed trapped surfaces extend into the region between the spherically symmetric trapping horizon and the event horizon. The surfaces we find here do the same.

In this article we will look at the variation of black hole parameters for horizons located on various different slicings of the same spacetime. We will examine several different spherically symmetric mass functions; a linear mass function designed to see the behaviour for slowing evolving black holes and a tanh log mass function, designed to see the behaviour in a short collapse of a shell to a black hole. We compare marginally outer trapped surfaces found on non-spherically symmetric hypersurfaces with those found on the spherically symmetric slicings. We are able to locate the spherically symmetric horizons analytically but the non-spherically symmetric horizons are located numerically using the AHFinderDirect thorn [23, 24] of the Cactus framework [25–27]. A number of useful analytic relations for the Vaidya spacetime are given in the appendix. Background detail on the properties of trapping horizons and their thermodynamics can be found in [1] and [3].

II. THE VAIDYA METRIC

To examine the slicing dependence of quasi-local horizons we need to consider dynamical spacetimes. The Vaidya solutions have a number of nice properties that make them popular for investigations of this type [19–21]. The Vaidya spacetimes [28] are a class of spherically symmetric, non-vacuum spacetimes with line element in advanced null Eddington-Finkelstein coordinates (v, r, θ, ϕ) :

$$ds^2 = - \left(1 - \frac{2m(v)}{r} \right) dv^2 + 2dvdr + r^2 d\theta^2 + r^2 \sin^2 \theta d\phi^2. \quad (1)$$

The function $m(v)$ is a freely specifiable mass function; it coincides with the Misner-Sharp mass [29] in this case. In advanced Eddington-Finkelstein coordinates the metric is well defined across future horizons. The Vaidya metric solves the Einstein equations with an energy-momentum tensor of the form

$$T_{ab} = E n_a n_b, \quad (2)$$

where n^a is an ingoing radial null direction and E is a function that depends on the normalization of n^a . For example, for the case where $n_a = -\partial_a v$ then we have

$$T_{ab} \ell^a \ell^b = \frac{\dot{m}}{4\pi r^2}, \quad (3)$$

when $n^a \ell_a = -1$ and defining $\dot{m} = \frac{dm(v)}{dv}$ which we will usually take to be positive definite, unless mentioned otherwise. The Vaidya solution can be interpreted as describing the radial collapse of pressureless null dust (i.e. infalling radiation). From the appendix we can see that, in a spherically symmetric foliation, trapping horizons will occur at $r = 2m(v)$ provided we keep $m(v) > 0$.

Here we will study various mass functions for $m(v)$. The simplest is a linear mass function of the form

$$m(v) = m_0 + \dot{m}v. \quad (4)$$

The linear mass function is suited to situations where the black hole is accreting matter at a constant rate (for a finite time duration to ensure that the mass stays finite). For the case $\dot{m} < 1/16$ the global Vaidya solution describes a naked singularity [30] but we are only interested here in the behaviour near the horizons and would in a real simulation assume some other metric is valid globally. While the assumption of spherical symmetry is somewhat artificial, real astrophysical black holes do have very small mass accretion rates whether from the accretion of surrounding stars and gas or purely from the accretion of photons from the cosmic microwave background. In the Vaidya solutions the Misner-Sharp mass on each ingoing constant v surface is a constant. This reflects the fact that the mass is flowing inwards at the speed of light and the mass contained within a shell of radius r is constant as the radius decreases. Although the spacetime is dynamical we can still define observers

who remain at a fixed areal radius r and fixed θ and ϕ . In terms of the proper time τ of such observers we have

$$\frac{dv}{d\tau} = \frac{1}{\sqrt{1 - 2m(v)/r}}. \quad (5)$$

At large distances from the black hole $r \gg m(v)$ we can use this to relate directly the mass flux in terms of the null coordinate v to the mass flux as seen by constant r, θ, ϕ observers who would be static observers in an exactly static spacetime,

$$\frac{dm(v)}{dv} \sim \frac{dm(v)}{d\tau}. \quad (6)$$

We can give a very rough indication of the order of magnitude for \dot{m} that might be expected for certain astrophysical cases. The Eddington rate is used to estimate the maximal rate at which infalling matter can be supported by its own radiation pressure and large, luminous black holes are typically found with luminosities between 10 and 100% of the Eddington limit [31]. For a black hole accreting at a tenth of the Eddington limit the dimensionless accretion rate is approximately [15]

$$\dot{m} \simeq 10^{-22} \left(\frac{M}{M_\odot} \right). \quad (7)$$

This is $\sim 10^{38}$ ergs per second for a solar mass black hole. The matter falling into the black hole is ten times the energy being emitted as light. Since this accretion is usually associated with a disk it will not be spherically symmetric. For a black hole accreting purely from the Cosmic Microwave Background, which is assumed to be isotropic, we have from the Stefan-Boltzmann law, approximately

$$\dot{m} \simeq 10^{-50} \left(\frac{T}{T_{3K}} \right)^4 \left(\frac{M}{M_\odot} \right)^2. \quad (8)$$

For a black hole whose dynamics are dominated by evaporation through Hawking radiation we have

$$\dot{m} \simeq -10^{-81} \left(\frac{M_\odot}{M} \right)^2. \quad (9)$$

For numerical purposes we will investigate evolutions with mass rates much higher than astrophysical rates, typically $\dot{m} \sim 0.01$. To the extent that $2\sqrt{|\dot{m}|} \ll 1$, the spherically symmetric trapping horizon will still be a slowly evolving horizon in the sense of [32]. We will also look at mass functions of the tanh log form, with $m(v) = 0$ for $v < 0$ and for $v > 0$

$$m(v) = \frac{m_0}{2} \left(1 + \tanh \left(\log \left(\frac{v}{T} \right) \right) \right) = \frac{m_0 v^2}{v^2 + T^2} \quad (10)$$

The first derivative of this tanh log mass function vanishes at $v = 0$. Therefore the metric and its first derivative are continuous at $v = 0$. For T and m_0 greater than

zero, this mass function models the collapse of a hollow spherical shell of matter $m(v=0) = 0$ that asymptotically settles down to an isolated black hole of mass m_0 for $v \rightarrow \infty$. These types of mass functions model situations where the black hole grows initially quite rapidly and then asymptotically settles down to its final static state. The mass function reaches half its asymptotic value when $v = T$.

The maximum of \dot{m} for these tanh log functions occurs at $v = T/\sqrt{3}$ and takes a value $\sim m_0/T$. Therefore these solutions will not be slowly evolving in the sense of [32] for m_0 and T of similar sizes.

A. Location of spherically symmetric horizons

Trapping horizons are three-dimensional surfaces H , foliated by closed spacelike two surfaces for which the future directed null normals ℓ^a and n^a satisfy

$$\theta_{(\ell)} = 0, \quad \theta_{(n)} < 0, \quad \mathcal{L}_n \theta_{(\ell)} < 0. \quad (11)$$

Here $\theta_{(\ell)}$ and $\theta_{(n)}$ are the expansions of ℓ^a and n^a respectively, and \mathcal{L}_n is the Lie derivative along n^a . Dynamical horizons are also three-dimensional surfaces foliated, as above, by spheres with $\theta_{(\ell)} = 0$, $\theta_{(n)} < 0$. However, $\mathcal{L}_n \theta_{(\ell)} < 0$ is replaced by the requirement that H be spacelike. For the spherically symmetric horizons in Vaidya, these notions coincide, provided $\dot{m} > 0$ [1].

For spherically symmetric slicings, the null normals associated with the trapping horizon will be radial null vectors and the location of the trapping horizon is just given by

$$r = 2m(v). \quad (12)$$

This is a spacelike surface for $\dot{m} > 0$, a null surface for $\dot{m} = 0$ and a timelike surface for $\dot{m} < 0$. For the linear mass function, in terms of the timelike coordinate $t = v - r$, the horizons will be located at

$$r = \frac{2m_0 + 2\dot{m}t}{1 - 2\dot{m}}. \quad (13)$$

For the tanh log mass function the horizons are located at the solution of the cubic

$$r^3 + (2t - 2m_0)r^2 + (t^2 + T^2 - 4m_0t)r - 2m_0t^2 = 0. \quad (14)$$

The equation for the horizon $r = 2m(v)$ has a single unique solution on each surface of constant v . But it can have multiple solutions, corresponding to multiple horizons, on surfaces of constant t . For $m_0 > 0$ this cubic function always has at least one positive real root and guarantees that there will always be at least one horizon. In fact, it can be shown that there will only be a single horizon for $t > 2m_0 - \sqrt{4m_0^2 - T^2}$. For small values of t there are multiple horizons and this will also be the case for other mass functions.

We will use numerical methods to solve the trapping horizon equations for non-spherically symmetric slicings and postpone discussion of them until the next section. Due to results in [4] we expect that the non-spherically symmetric trapping horizons will intersect the spherically symmetric ones.

The event horizons are defined as the past causal boundary of future null infinity and are generated by null geodesics that fail to reach infinity. The event horizon is always a null surface since it is a causal boundary. In the Vaidya spacetimes it is generated by radial outgoing null vectors that satisfy

$$\frac{dr}{dv} = \frac{1}{2} \left(1 - \frac{2m(v)}{r} \right). \quad (15)$$

This first order ordinary differential equation generates the path of all outgoing radial null geodesics. In order to give the location of the event horizon it requires a boundary condition that corresponds to the known location of the event horizon at some particular point. In practice this is usually given by the position of the event horizon at some future point, either when the black hole evaporates entirely or settles down to a stationary state. If the black hole at some point settles down to a Schwarzschild black hole with no further matter accreting, then the event horizon can be located by tracing back the null rays from the future Schwarzschild radius. However, in the situation where the black hole is accreting matter at a steady rate and is a suitably long way from changing this accretion rate one can find the approximate location of the event horizon by imposing the condition

$$\frac{d^2r}{dv^2} = 0. \quad (16)$$

This just reflects the fact that the event horizon is growing at a steady rate [15]. Imposing this condition on equation (15) gives the general solution

$$r = \frac{m(v)}{4\dot{m}} \left(1 - \sqrt{1 - 16\dot{m}} \right). \quad (17)$$

For $|\dot{m}| \ll 1$ this gives

$$r = 2m(v) (1 + 4\dot{m} + \mathcal{O}(\dot{m}^2)) \quad (18)$$

and thus we expect that the event horizon will be outside the spherically symmetric trapping horizon for $\dot{m} > 0$ but inside for $\dot{m} < 0$. For a solar-mass black hole accreting at a tenth of the Eddington rate the difference in areas between the event horizon and the spherically symmetric trapping horizon will be around 10^{56} in units of Planck area, while for a supermassive black hole of mass 10^8 solar masses, accreting purely from the CMB, the difference in areas will be around 10^{60} in Planck units [15]. In terms of the coordinate $t = v - r$ for the linear mass function the event horizon has radial coordinate

$$r \sim \frac{2m + 2\dot{m}t}{1 - 2\dot{m}} + \frac{8m\dot{m}}{1 - 2\dot{m}}. \quad (19)$$

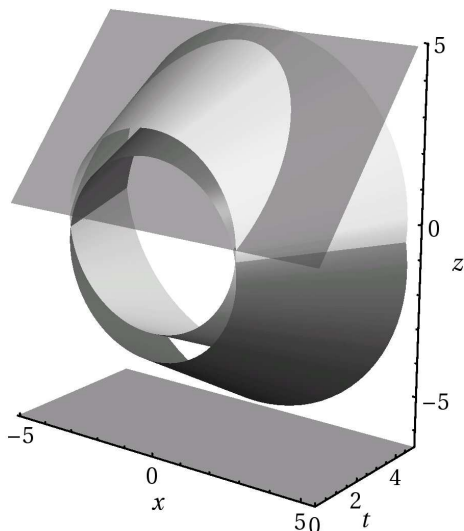


FIG. 1. Two trapping horizons in the Vaidya spacetime. A three-dimensional projection, with the y coordinate – equivalently θ coordinate – suppressed, of the Vaidya spacetime with $m(v) = 1.0 + 0.15v$, showing the growing trapping horizons corresponding to the spherically symmetric horizon (light grey tube) and to the $\bar{t}_{\alpha=0.9}$ -slicing (dark grey tube). The transparent planar surface is the $\bar{t}_{\alpha=0.9} = 0$ slice.

This is just the location of the spherically symmetric trapping horizon with a constant offset of $8m\dot{m}$ provided $|\dot{m}| \ll 1$. In this approximation the generators of both the trapping horizon and the event horizon have the same components but the norm of the generators is $4\dot{m}$ for the trapping horizon and zero for the event horizon.

B. An axisymmetric spacetime slicing

We consider a simple axisymmetric slicing of the form

$$\bar{t} = v - r - \alpha z, \quad (20)$$

where $z = r \cos \theta$ and α is a parameter that determines how far away from spherical symmetry the constant \bar{t} surface is. We reserve the symbol t for spherically symmetric surfaces where $\alpha = 0$, which just gives the usual Eddington-Finkelstein time coordinate (although not the Schwarzschild time coordinate). Hypersurfaces of constant \bar{t} are always spacelike for $|\alpha| < 1$ since the normal to a given hypersurface, \bar{t}^a , has norm

$$\bar{t}^a \bar{t}_a = \alpha^2 - 1 - \frac{2m(v)}{r} (1 + \alpha \cos \theta + \alpha^2 \cos^2 \theta). \quad (21)$$

On the slice $\bar{t} = 0$ we have $v > 0$ everywhere for $|\alpha| < 1$. In addition, since $(1 + \alpha \cos \theta + \alpha^2 \cos^2 \theta)$ is always greater than $3/4$, for real α this hypersurface will become timelike near the horizon for $\alpha > \sqrt{7}/2 \sim 1.323$.

On each slice with a constant value of \bar{t} , a two dimensional marginally outer trapped surface (MOTS) can be

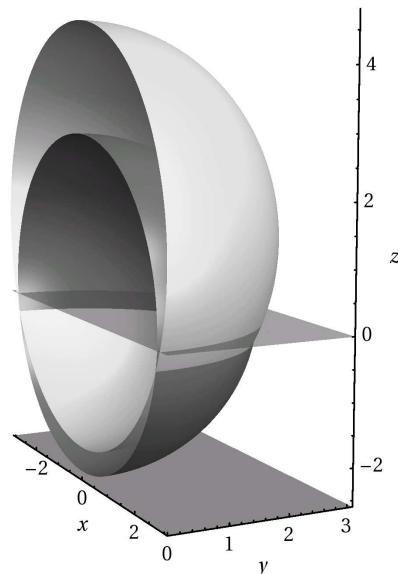


FIG. 2. The $\bar{t}_{\alpha=0.9} = 0$ hypersurface of a Vaidya spacetime with $m(v) = 1.0 + 0.15v$, showing the MOTS that lies on this slice (dark grey sphere) and the intersection (light grey sphere) of the $\alpha = 0$ trapping horizon passing through this slice. The dark grey sphere is not a MOTS itself, but is made up of points that lie on many different MOTS of the spherically symmetric trapping horizon. The transparent plane intersecting the two spheres is the equatorial plane $z = 0$ which lies on both $\bar{t} = 0$ hypersurfaces and $t = 0$ hypersurfaces.

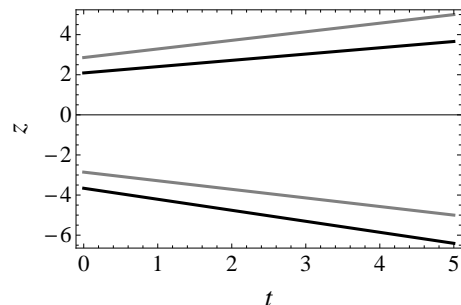


FIG. 3. (t, z) -plane of Fig.1 showing the t -evolution of the north poles (positive z) and south poles (negative z) of the spherically symmetric trapping horizon (light grey) and the $\bar{t}_{\alpha=0.9}$ -trapping horizon (dark grey). For these points z is the same as the radial coordinates r .

searched for, satisfying just $\theta_{(\ell)} = 0$. In some spacetimes there may be multiple MOTS on a given hypersurface. This will not occur in the Vaidya spacetimes with linear mass function since the horizon condition, $r = 2m(v)$, is linear in r . The marginally outer trapped surfaces can typically be stacked to form three dimensional trapping horizons, provided the other conditions $\theta_{(n)} < 0$ and $n^a \nabla_a \theta_{(n)} = 0$ are satisfied too (or a dynamical horizon if the resulting surface is spacelike).

For the case $\alpha = 0$ the slicings will be spherically symmetric. The orbit of spherical rotations of each point will lie entirely in the hypersurface. This will lead to MOTS

that are spherically symmetric, where each surface is just the orbit of spherical rotations. Commonly used slicings in numerical relativity such as constant mean curvature surfaces will typically be spherically symmetric in the Vaidya spacetime. In this case the horizons will be located uniquely at $r = 2m(v)$ and every point on the surface will have the same value of the advanced time v . This will not be the case for surfaces with $\alpha \neq 0$. In these cases the mass parameter $m(v)$ will not necessarily take the same value on different points of the surface. The MOTS will then extend into regions where the matter is more compact and regions where it is less compact. Surfaces with $\alpha > 0$ will be the same as surfaces with $\alpha < 0$, with the north pole ($\theta = 0$) interchanged with the south pole ($\theta = \pi$) or, equivalently $\cos\theta \rightarrow \cos(\pi - \theta)$.

Each different choice of \bar{t} will lead to different MOTS that can be stacked to form different trapping horizons. Each of these trapping horizons will have an associated natural foliation, the one that makes each two dimensional surface a MOTS. However we can also consider the intersection of a given trapping horizon with a space-like hypersurface of a given α value different from the one that foliates it into MOTS. We can compute the area of these two surfaces, although they are not MOTS. For the spherically symmetric trapping horizon (SSTH) in Vaidya spacetime with linear mass function and $|\dot{m}| \ll 1$, the area will be

$$A_{\text{SSTH}} = 4\pi (2m)^2 \left(1 + 4\dot{m} + 2\dot{m} \frac{\bar{t}}{m} + \frac{4}{3} \dot{m} \alpha^2 \right). \quad (22)$$

A similar calculation can be performed for the intersections of the event horizon with the constant \bar{t} surfaces. Taking the position of the event horizon to be (18) and again the approximation $|\dot{m}| \ll 1$ we find

$$A_{\text{EH}} = 4\pi (2m)^2 \left(1 + 12\dot{m} + 2\dot{m} \frac{\bar{t}}{m} + \frac{4}{3} \dot{m} \alpha^2 \right). \quad (23)$$

If we compare the area of the event horizon on a constant \bar{t} hypersurface with the area of the event horizon on a spherically symmetric surface with $\alpha = 0$ but the same constant value of t we see that the area will be greater if $\dot{m} > 0$ and smaller if $\dot{m} < 0$.

C. Horizon deformations

The choice of different foliations leads to different MOTS that can be deformed into each other. Using these deformations it is possible to examine how certain geometric properties of surfaces change with the deformation [33]. For example, it is possible to see how the area element, ϵ , changes as MOTS are deformed into one another.

We can search for MOTS on slices with different values of \bar{t} but because these marginally trapped surfaces do not lie on the same hypersurface it is difficult to compare them. If the MOTS do not intersect (and typically they

don't) it may not be possible to find a trapping horizon that connects both surfaces. We want to distinguish between marginally trapped surfaces that are evolutions of one another and marginally trapped surfaces that cannot be evolved into one another along a trapping horizon.

For a given choice of \bar{t} but two different values of α the two slices thus defined will intersect when $z = 0$. The slice $t = 0$ with $\alpha = 0$ does not lie entirely to the past or future of the slice $\bar{t} = 0$ with $\alpha = 1$. However, the horizons on these two slices will typically not intersect. On the two dimensional surface where these two slices do intersect, $z = 0$, the horizon for $\alpha = 0$ is found to lie outside the horizon with $\alpha \neq 0$.

For a given surface, a given infinitesimal deformation of that surface can be defined by a vector field X . Variation of a quantity Q with respect to this deformation can then be written as $\delta_X Q$. Following [32] we can write this vector field on a marginally trapped surface in terms of the two null normals to the surface as

$$X^a = B\ell^a - Cn^a, \quad (24)$$

where B and C are functions on the surface. The minus sign in the above is chosen in the literature because when the deformation vector generates evolution along a spacelike dynamical horizon, both B and C are positive. For deformations of the spherically symmetric surface, where $\Delta = 0$ as defined in the appendix, we have

$$X^a = B \frac{\partial}{\partial v} + C \frac{\partial}{\partial r} \quad (25)$$

for the Eddington-Finkelstein coordinates v and r . The variation of intrinsic geometrical scalar properties can be calculated using

$$\delta_X \phi = \mathcal{L}_X \phi, \quad (26)$$

and for general tensors, by projecting the Lie derivative onto the surface

$$\delta_X w_{ab} = q_a^c q_b^d \mathcal{L}_X w_{cd}. \quad (27)$$

The variation of the area element ϵ for example satisfies

$$\delta_X \epsilon = -C\theta_{(n)}\epsilon. \quad (28)$$

Variations of extrinsic properties are a little harder to calculate. We are particularly interested in deformations of the form

$$\delta_X \theta_{(\ell)} = 0, \quad (29)$$

since this will generate a class of marginally outer trapped surfaces. The calculations in [32] give

$$\delta_X \theta_{(\ell)} = -d^2 C + 2\tilde{\omega}^a d_a C - C\delta_n \theta_{(\ell)} + B\delta_\ell \theta_{(\ell)}, \quad (30)$$

where d is the covariant derivative compatible with the intrinsic metric of the two-surface and $\tilde{\omega}^a$ is given in the appendix and defined in [32]. From [32] we also have

$$\delta_n \theta_{(\ell)} = -\frac{\tilde{R}}{2} + \|\tilde{\omega}\|^2 - d_a \tilde{\omega}^a + 8\pi T_{ab} \ell^a n^b, \quad (31)$$

$$\delta_\ell \theta_{(\ell)} = -\|\sigma_{(\ell)}\|^2 - 8\pi T_{ab} \ell^a \ell^b, \quad (32)$$

where again the various terms are given in the appendix. For radial ℓ^a we have (3) and thus

$$\delta_\ell \theta_{(\ell)} = -\frac{2\dot{m}}{r^2}, \quad (33)$$

since the shear is zero. Axisymmetric variations from the spherically symmetric surface will satisfy

$$-\frac{d^2 C}{d\theta^2} - \cot\theta \frac{dC}{d\theta} + C - 2\dot{m}B = 0. \quad (34)$$

In the case where both B and C are constant we get the evolution along the spherically symmetric trapping horizon. In [32] it was assumed that the deformations were *l-oriented* such that $B > 0$ everywhere. In general solutions of (34) can be decomposed into Legendre polynomials. The simplest non-trivial solution of this equation is based on the $n = 1$ Legendre polynomial,

$$B = k \cos\theta, \quad (35)$$

$$C = \frac{2\dot{m}}{3} k \cos\theta, \quad (36)$$

where k is a constant of integration. Since the variation in this case is dependent on θ it will not generate spherically symmetric marginal surfaces, and since $B = C = 0$ for $\theta = \pi/2$ this will not generate evolution along a trapping horizon as there are fixed points under the deformation. The area change in this case is easily computed as

$$\int \delta_X \epsilon = - \int C \theta_{(n)} \epsilon = \frac{4\dot{m}k}{3r} \int \cos\theta \sin\theta d\theta d\phi = 0. \quad (37)$$

In this case, at least, the area of the spherically symmetric surface is extremal with respect to this deformation. That this is also true for deformations comprised of higher degrees of the Legendre polynomials follows simply, for example, from the orthogonality property of the Legendre polynomials.

III. NUMERICAL RESULTS FOR AXISYMMETRIC SLICINGS

We now compare the different trapping horizons one obtains for the axisymmetric slicings given by (20) where we consider the linear mass function (4) and tanh log mass function (10). The results are qualitatively similar for a range of values \dot{m} and α and we will display results for several different values of these parameters. For the numerical calculation in the following we use, as in previous work [19], the Cactus computational toolkit [25, 26] which is widely used in numerical relativity, for example to perform binary black hole, neutron star, or stellar core collapse simulations. For a given slicing \bar{t}_α we write the corresponding induced 3-metric of Vaidya

on a $\bar{t}_{\alpha=\text{const}}$ slice using the Cartesian grid of Cactus. To locate the trapping horizon on each slice we use the apparent horizon finder AHFinderDirect [23, 24]. This way we obtain the location and area of the trapping horizon as a function of \bar{t}_α -time. In the following we compare these functions for the different trapping horizons we detect on the axisymmetric slicings from above.

A. Location of tilted versus untilted horizons

A trapping/dynamical horizon is obtained by stacking together a sequence of MOTS on successive spatial slices. This results in a three-dimensional surface embedded in a four dimensional spacetime. This can be difficult to visualize. We can display the horizons graphically in a three dimensional plot by suppressing an angular coordinate. Figure (1) shows two particular horizons corresponding to the spherically symmetric $\alpha = 0$ and the non-symmetric $\alpha = 0.9$ slicings. The MOTS and their horizons are displayed in Figures (1) and (2). Figure (1) shows two different trapping horizons obtained from stacking MOTS of $\alpha = 0$ slicings and $\alpha = 0.9$ slicings respectively. The horizons intersect just below the equator $z = 0$. In this three-dimensional plot the θ coordinate has been suppressed.

Figure (2) shows the points lying on the planar surface shown in Figure (1), now restoring the θ dependence but with \bar{t} everywhere zero. Figure (2) displays the MOTS of the $\bar{t} = 0$ slice with $\alpha = 0.9$ and the intersection of the spherically symmetric trapping horizon with this $\bar{t} = 0$ hypersurface. It should be emphasized that this intersection is however not itself a MOTS.

Figure (3) shows the evolution in time of the north and south poles of the individual MOTS. Effectively this figure corresponds to a slice through Figure (1) at $x = 0$. It shows that the north pole of the spherically symmetric trapping horizon is outside the north pole of the tilted, $\bar{t} = 0$ trapping horizon and the south pole of the spherically symmetric trapping horizon is inside the south pole of the tilted, $\bar{t} = 0$ trapping horizon.

The MOTS lying on the hypersurfaces $\bar{t} = v - r - \alpha z = 0$ with different values of α do not intersect. An examination of the marginally outer trapped surface with $\alpha = 0.83$ shows that the points at the north pole $\theta = 0$, on the equator $\theta = \pi/2$ and at the south pole $\theta = \pi$ have the four-dimensional spacetime coordinates given in Table (I)

TABLE I. Coordinate location of various points on surface with $\bar{t} = 0$, $\alpha = 0.83$ and $m(v) = 1.0 + 0.01v$

surface point	r	v	t
zmax (north pole)	2.0454	3.7498	1.7044
xmax (equator)	2.0386	2.0386	0.0000
zmin (south pole)	2.0247	0.3374	-1.6872

Trapping horizons can be formed by stacking surfaces found on different hypersurfaces with different values of \bar{t} but the same value of α . One can obtain a trapping horizon in this manner for each value of α . These trapping horizons, each with their own value of α will intersect one another. This can also be seen in Table (I). The points on the equator lie inside the horizon located on the spherically symmetric slicing $t = v - r = 0$, where every point on the horizon has $r = 2.0408$ and $t = 0$. The point at the north pole lies inside the spherically symmetric horizon on the slice $t = 1.7044$, which lies at $r = 2.0756$, and the point at the south pole lies outside the spherically symmetric horizon on the slice $t = -1.6872$, which lies at $r = 2.0064$.

The area of the MOTS with values given in Table (I) is 52.3359. The various points of this MOTS can be compared with spherically symmetric MOTS on surfaces of constant v or t for the coordinate values found, using the formula given in (13). For the north pole, the area of the spherically symmetric MOTS with $t = 1.7044$ has area 52.3381 and the area of the spherically symmetric MOTS with $v = 3.7498$ has area 54.1059. For the south pole, the area of the spherically symmetric MOTS with $t = -1.6872$ has area 50.5869 and the area of the spherically symmetric MOTS with $v = 0.3374$ has area 50.6052. Since the area of the MOTS with values given in Table (I) is 52.3359, we see that the corresponding spherically symmetric MOTS with the maximum values of t and v have greater area than the tilted $\bar{t} = 0$ MOTS described and the corresponding spherically symmetric MOTS with the minimum values of t and v have lesser area. This is likely to be true for any value of α and \bar{t} provided $\dot{m} > 0$.

In terms of the deformations discussed above (25) we see that to deform the spherically symmetric surface at $t = 0$ we need $B > 0$ and $C > 0$ at the north pole and $B < 0$ and $C < 0$ at the south pole, where in both cases the size of C is much smaller than B .

Figure (4) shows the locations (r coordinate) of the north pole, equator and south poles for MOTS against α for a mass function of the form $m(v) = 1.0 + 0.01v$. For values of α less than zero the location of the MOTS is the same with the north pole $\theta = 0$ and south pole $\theta = \pi$ interchanged. Near the spherically symmetric MOTS at $\alpha = 0$ the change in the r coordinate of the equator is zero. This can be seen in Figure (4) and is true by the reflection symmetry around $\alpha = 0$ although the second rate of change of r with respect to α may not be zero at this point. The change in the r coordinates of the north and south poles is equal but opposite in sign. We may conjecture that the variation of the surface near $\alpha = 0$ is given by (35) and (36) in (25). The numerical results obtained here are consistent with this conjecture being true, although the results are also consistent with the power being dominated by any odd degree Legendre polynomial.

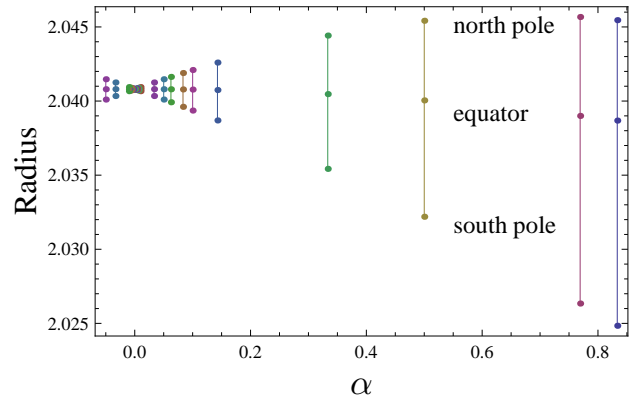


FIG. 4. The location (r -coordinate) of the north pole, equator and south pole versus different values of α for a linear mass function $m(v) = 1.0 + 0.01v$. The positions for negative α are the same as for positive α with the north pole and south pole interchanged. Near $\alpha = 0$ there is no change in the position of the equator and the change in the position of the north pole and south pole are equal but opposite in sign.

B. Area dependence on α

The results for the area dependence of α are shown in the upper panel of Fig.(5) for the linear mass case and the lower panel of Fig.(5) for the tanh log mass function. The $\alpha = 0$ surfaces have the largest area. As expected the area of the tilted horizons is unchanged under a change in sign of α . The difference between the area on $\alpha = 0$ slices and $\alpha \neq 0$ slices depends on \dot{m} as shown in Fig.(6) for the linear mass function. It is zero for $\dot{m} = 0$, where the spacetime just reduces to the Schwarzschild solution and the horizon is an isolated horizon. The difference between the area of tilted and untilted horizons increases with increasing magnitude of \dot{m} . The difference is slightly larger for positive values of \dot{m} than for negative values. This difference in area does not seem to follow a simple power law and it is difficult to extrapolate what the difference in areas will be for values of \dot{m} different from the values examined. However, the difference in areas for values of \dot{m} much lower than the lowest positive value of \dot{m} considered here ($\dot{m} = 0.02$) are likely to be much less than the $\sim 0.017\%$ difference found here for that case.

Finally, Fig. 7 compares the area of the event horizon (or more precisely, the intersection of the event horizon with the spatial slices corresponding to different values of α) with the area of the MOTS as functions of α . It is interesting that the variation in the event horizon area, plotted against the left hand axis, is much larger than for the apparent horizon, plotted against the right hand axis.

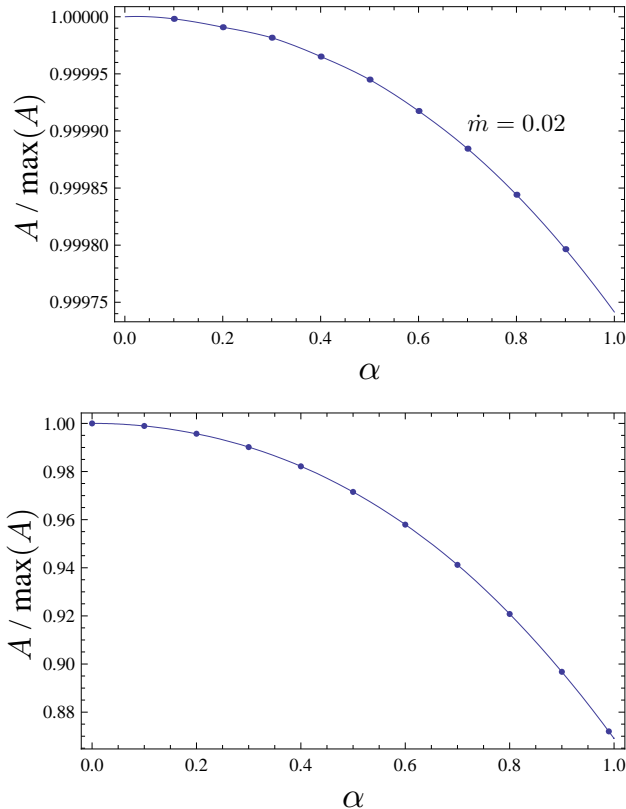


FIG. 5. Slicing dependence of the area at $\bar{t} = 0$ for the linear mass function (top) with $m = 1.0$ and $\dot{m} = 0.02$ and for the tanh log mass function (bottom) with $m = 1.0$ and $T = 1.0$

C. Dependence of rate of change of area on α

For the linear mass function the $\alpha \neq 0$ surfaces seem to have the same rate of change of area as the $\alpha = 0$ surfaces, at least to within numerical accuracy. For the tanh log mass function, as depicted in Fig.(8), the area of tilted horizons grows at a greater rate than the untilted areas and both converge to the asymptotic isolated horizon area, which will also be the asymptotic area of the event horizon. In this sense the spherically symmetric trapping horizon plays a special role as it is the one with the smallest rate of increase of area. This would seem to contradict the conjecture made in [34] that the preferred trapping horizon should be the one where the area increases the most and approaches the event horizon the fastest. However, it is not known whether this behaviour is repeated in more general situations with other mass functions or other slicing conditions.

IV. CONCLUSION AND DISCUSSION

We have investigated the slicing dependence of the apparent horizons in the Vaidya spacetime. For a given slice

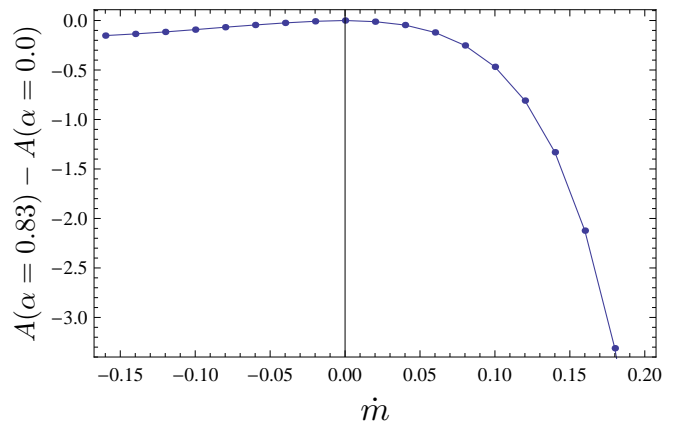


FIG. 6. Area difference for two slices in different Vaidya spacetimes with linear mass function and $m = 1.0$, The difference between the areas increases for large \dot{m} . The untilted areas are larger than the tilted areas for \dot{m} both positive and negative. However, the difference is much larger for $\dot{m} > 0$. Only for $\dot{m} = 0$ do the areas coincide.

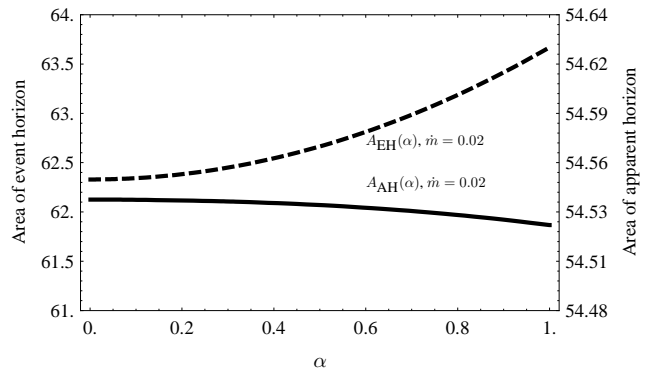


FIG. 7. Area of the event horizon A_{EH} (dashed line) and the MOTS A_{AH} for different values of α for the linear mass function with $\dot{m} = 0.02$. The y-axis on the left refers to the area of the event horizon and the axis on the right to the area of the apparent horizon; the scale of A_{AH} has been expanded to better show its variation. The variation of A_{EH} is much larger than the variation of A_{AH} and the variation of A_{AH} is small relative to the difference between A_{EH} and A_{AH} .

we have looked at three types of horizons; the MOTS that lie on the slice, the intersection of the slice with the event horizon and the intersection of the slice with the spherically symmetric trapping horizon. We have examined rather simple axisymmetric slicings in this simple spacetime. These simple slicings do not exhaust all possible axisymmetric slicings and there are many other possible slicings that are not axisymmetric.

Explicitly the location of the horizons is different for different choices of horizon and different choices of slicing. However, for slowly evolving horizons, the areas do not vary by much, although the larger the rate at which the black hole accretes matter the larger the difference in the areas. For the $\dot{m} = 0.02$ Vaidya solution with linear mass

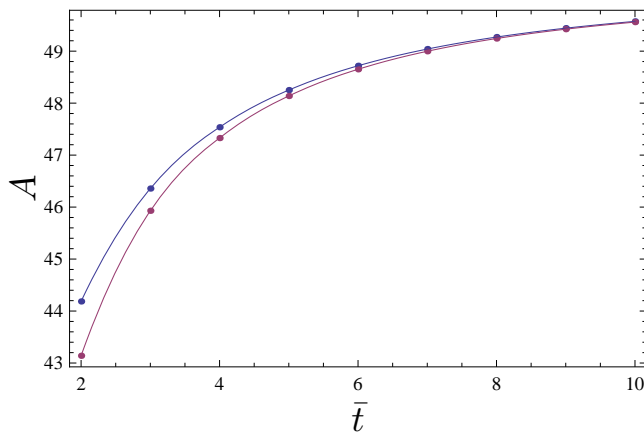


FIG. 8. Area versus time \bar{t} for $\alpha = 0$ and $\alpha = 0.83$ for the tanh log mass function with $m = 1.0$ and $T = 1.0$. Both areas converge rapidly to the asymptotic isolated horizon area 16π . The tilted area grows faster since it starts from a lower point.

function the area can vary by approximately 0.03% as α is varied from 0 to 1. Beyond $\alpha = 1$ the Cauchy surface becomes timelike for certain values of θ . This value, $\dot{m} = 0.02$, is still much larger than the mass accretion rate expected for astrophysical black holes.

From a purely practical point of view we’ve found evidence that the parameters of the black hole, derived from its trapping horizon, do not change significantly when looking at reasonably simple slicings. It is still unknown whether the properties would change drastically for certain unusual slicings, but these are unlikely to occur in normal numerical simulations. It is also reassuring that these differences are much smaller than the parameter biases of up to 10% found between different post-Newtonian models [14]. This variation of the parameters with foliation will also occur if one uses the event horizon.

From a conceptual point of view, we have demonstrated explicitly the known result that the location of the black hole surface and some of its properties such as the area depend on the choice of the spacetime slicing. There are a variety of different possible responses to the issue of non-uniqueness of the trapping horizons in a given spacetime. The oldest approach is to focus purely on the event horizon as the unique indicator of the black hole and its properties. The location of the event horizon is independent of the choice of foliation. This approach however causes trouble in certain quantum inspired spacetimes [3, 18] where no event horizon exists. In numerical settings, the teleological definition of the event horizon means that it is only known after a simulation is finished, preventing it from being used to analyse the simulation’s state as it proceeds.

Another approach is to accept all horizons on an equal footing as purely a property of the geometry. In this picture it is not clear how to associate unique properties to the black hole such as a horizon area or horizon angular momentum. Because the horizons intersect one cannot rely on specifying, for example, the outermost trapping

horizon. However, it may be possible to formulate a generalized second law for each possible foliation of spacetime and in this context use the horizon defined by the chosen foliation.

A third approach is to look for the boundary of the region that admits trapped surfaces. This surface should be spherically symmetric in a spherically symmetric spacetime. If this surface lies strictly outside the spherically symmetric trapping horizon then, by the results of [4], it cannot itself admit the structure of a dynamical horizon. This surface will have a location that is independent of any given foliation, although it may not have a simple thermodynamic interpretation.

A fourth approach is to look for properties that select out a certain preferred trapping horizon in the spacetime [35], such as the spherically symmetric horizon in a spherically symmetric spacetime. This would require some additional condition to be imposed that selects out a unique trapping horizon from the many that occur in dynamical black hole spacetimes. One possibility displayed here is the horizon that locally maximises the area of MOTS under small deformations.

Despite their quasi-local nature, closed marginally trapped surfaces do have some non-local behaviour. Their dependence on the slicing is but one manifestation of this behaviour. The fact that marginally outer trapped surfaces can be found all the way to the event horizon [20] is another manifestation. Although the event horizon is a fully non-local teleologically defined surface, it still acts as the boundary of outer trapped surfaces in a Vaidya spacetime that satisfies the null energy condition and asymptotes to a static Schwarzschild solution in the far future.

This behaviour is related to both the choice of the surface null normals and the requirement that the marginally trapped surface be closed. Closed trapped surface cannot be found entirely in a flat spacetime. However, parts of a closed marginally trapped surface can be found passing through a region of flat space where both null expansions are negative [21].

It may be that in the quantum context only an effective horizon is meaningful or that the existence of many intersecting horizons contribute to the full path integral. For purely classical situations one may be able to refine the definition of the surface of a black hole.

V. APPENDIX – SOME USEFUL RELATIONS IN THE VAIDYA SPACETIME

These relations are provided here as a repository for reference in the main text. In the advanced null Eddington-Finkelstein coordinates (v, r, θ, ϕ) the metric takes the form

$$ds^2 = -\Delta dv^2 + 2drdv + r^2 d\Omega^2, \quad (38)$$

where $\Delta = 1 - \frac{2m(v)}{r}$, $\Delta' = \frac{2\dot{m}(v)}{r^2}$, $\dot{\Delta} = -\frac{2\dot{m}}{r}$ and $\dot{m} = \partial_v m(v)$.

Radial null vectors, with canonical normalization $\ell^a n_a = -1$ and $n_a = -\partial_v r$:

$$\ell^a = \left(1, \frac{\Delta}{2}, 0, 0\right), \quad (39)$$

$$\ell_a = \left(-\frac{\Delta}{2}, 1, 0, 0\right), \quad (40)$$

$$n^a = (0, -1, 0, 0), \quad (41)$$

$$n_a = (-1, 0, 0, 0). \quad (42)$$

Expansions of the null normals:

$$\theta_{(\ell)} = \frac{\Delta}{r}, \quad \theta_{(n)} = -\frac{2}{r}. \quad (43)$$

The location of the spherically symmetric MOTS is obtained by setting $\theta_{(\ell)} = 0$ leading to $r = 2m(v)$. The variations of the expansions along n^a :

$$n^a \nabla_a \theta_{(\ell)} = \frac{\Delta}{r^2} - \frac{\Delta'}{r}, \quad (44)$$

$$\ell^a \nabla_a \theta_{(\ell)} = \frac{\dot{\Delta}}{r} - \frac{\Delta^2}{2r^2} + \frac{\Delta \Delta'}{2r}, \quad (45)$$

$$n^a \nabla_a \theta_{(n)} = -\frac{2}{r^2}, \quad (46)$$

$$\ell^a \nabla_a \theta_{(n)} = \frac{\Delta}{r^2}. \quad (47)$$

Other optical scalars:

$$\sigma_{(\ell)} = \sigma_{(n)} = \omega_{(\ell)} = \omega_{(n)} = 0. \quad (48)$$

Surface gravities:

$$\kappa_{(\ell)} = -n^a \ell^b \nabla_b \ell_a = \frac{\Delta'}{2}, \quad (49)$$

$$\kappa_{(n)} = -\ell^a n^b \nabla_b n_a = 0. \quad (50)$$

Components of the energy-momentum tensor:

$$T_{ab} = \frac{\dot{m}}{4\pi r^2} n_a n_b, \quad (51)$$

$$T_{ab} \ell^a \ell^b = \frac{\dot{m}}{4\pi r^2}, \quad (52)$$

$$T_{ab} n^a \ell^b = T_{ab} n^a n^b = 0. \quad (53)$$

Normal to the trapping horizon $\Delta = 0$:

$$N^a = (1, -2\dot{m}, 0, 0), \quad (54)$$

$$N_a = (-2\dot{m}, 1, 0, 0). \quad (55)$$

Radial tangent to the trapping horizon

$$V^a = (1, 2\dot{m}, 0, 0), \quad (56)$$

$$V_a = (2\dot{m}, 1, 0, 0). \quad (57)$$

Variation of the area along the trapping horizon

$$V^a \nabla_a A = \frac{4A\dot{m}}{r}. \quad (58)$$

Connection on the normal cotangent bundle

$$\tilde{\omega}_a = -\tilde{q}_a^b n_c \nabla_b \ell^c = (0, 0, 0, 0). \quad (59)$$

Scalar curvature of the horizon

$$\tilde{R} = \frac{2}{r^2}. \quad (60)$$

The null energy condition is satisfied if $\dot{m} > 0$. This is easy to see in a fiducial spherically symmetric null tetrad $\ell^a, n^a, m^a, \bar{m}^a$ since for a general null vector v^a with

$$v^a = A\ell^a + Bn^a + Cm^a + \bar{C}\bar{m}^a, \quad (61)$$

then $T_{ab} v^a v^b = A^2 T_{ab} \ell^a \ell^b = \frac{\dot{m}}{4\pi r^2} A^2 (\ell^a n_a)^2$. The null energy condition is closely related to whether there is positive or negative energy flowing into the black hole.

If $\dot{m} \neq 0$ there are no isolated horizons in the Vaidya spacetime since the norm of the generalized null vector (61) is

$$v^a v_a = -2AB + 2C\bar{C} = 0. \quad (62)$$

For this null vector to be the generator of an isolated horizon it is required to satisfy $T_{ab} v^a v^b = 0$ giving $A = 0$ and therefore from above $C = 0$. Thus any null vector generating an isolated horizon must be proportional to $\theta_{(n)}$ but from above we see $\theta_{(n)} = -2/r$. This only vanishes at infinity. There is a degenerate planar horizon at infinity.

VI. ACKNOWLEDGMENTS

Alex Nielsen gratefully acknowledges financial support from the Alexander von Humboldt Foundation and hospitality at the Albert Einstein Institute; Erik Schnetter acknowledges support from the NSF awards 0701566, 0721915, and 0904015. The numerical solutions were found using the AHFinderDirect thorn [23, 24] of the Cactus framework [25, 26] as part of the Einstein Toolkit [27]. We also thank Alberto Sesana, Jose Luis Jaramillo and Frank Ohme for helpful discussions.

During the work for this paper we were saddened to hear of the passing of Professor P. C. Vaidya, upon whose solution this work is based.

-
- [1] A. Ashtekar and B. Krishnan, Living Rev. Rel. **7** (2004) 10 [arXiv:gr-qc/0407042].
- [2] I. Booth, Can. J. Phys. **83** (2005) 1073 [arXiv:gr-qc/0508107].
- [3] A. B. Nielsen, Gen. Rel. Grav. **41** (2009) 1539 [arXiv:0809.3850 [hep-th]].
- [4] A. Ashtekar and G. J. Galloway, Adv. Theor. Math. Phys. **9** (2005) 1 [arXiv:gr-qc/0503109].
- [5] A. Ashtekar and B. Krishnan, Phys. Rev. D **68**, 104030 (2003) [arXiv:gr-qc/0308033].
- [6] I. Hinder, Class. Quant. Grav. **27**, 114004 (2010) [arXiv:1001.5161 [gr-qc]].
- [7] A. Buonanno, G.B. Cook, and F. Pretorius, Phys. Rev. D **75** (2007) 124018
- [8] J.G. Baker et al., Phys. Rev. Lett. **99** (2007) 181101
- [9] M. Campanelli et al., Phys. Rev. D **79** (2009) 084010
- [10] M. Boyle et al., Phys. Rev. D **76** (2007) 124038
- [11] M. Hannam et al., Phys. Rev. D **77** (2008) 044020
- [12] I. Hinder, F. Herrmann, P. Laguna and D. Shoemaker, Phys. Rev. D **82** (2010) 024033 [arXiv:0806.1037 [gr-qc]].
- [13] L. Santamaria et al., Phys. Rev. D **82** (2010) 064016 [arXiv:1005.3306 [gr-qc]].
- [14] A. Buonanno et al., Phys. Rev. D **80** (2009), 084043
- [15] A. B. Nielsen, Class. Quant. Grav. **27** (2010) 245016 [arXiv:1006.2448 [gr-qc]].
- [16] I. Booth and J. Martin, Phys. Rev. D **82** (2010) 124046 [arXiv:1007.1642 [gr-qc]].
- [17] W. A. Hiscock, Phys. Rev. D **23** (1981) 2813.
- [18] S. A. Hayward, Phys. Rev. Lett. **96** (2006) 031103 [arXiv:gr-qc/0506126].
- [19] E. Schnetter and B. Krishnan, Phys. Rev. D **73** (2006) 021502 [arXiv:gr-qc/0511017].
- [20] I. Ben-Dov, Phys. Rev. D **75** (2007) 064007 [arXiv:gr-qc/0611057].
- [21] I. Bengtsson and J. M. M. Senovilla, Phys. Rev. D **79** (2009) 024027 [arXiv:0809.2213 [gr-qc]].
- [22] J. E. Aman, I. Bengtsson and J. M. M. Senovilla, J. Phys. Conf. Ser. **229** (2010) 012004 [arXiv:0912.3691 [gr-qc]].
- [23] J. Thornburg, Phys. Rev. D **54** (1996) 4899 [arXiv:gr-qc/9508014].
- [24] J. Thornburg, Class. Quant. Grav. **21** (2004) 743 [arXiv:gr-qc/0306056].
- [25] T. Goodale, G. Allen, G. Lanfermann, J. Massó, T. Radke, E. Seidel and J. Shalf, “*The Cactus Framework and Toolkit: Design and Applications*,” Vector and Parallel Processing – VECPAR’2002, 5th International Conference, Lecture Notes in Computer Science, (2003), Springer, Berlin, url = <http://edoc.mpg.de/3341>,
- [26] Cactus Computational Toolkit, <http://www.cactuscode.org>
- [27] Einstein Toolkit, <http://einsteintoolkit.org>
- [28] P. C. Vaidya, Phys. Rev. **83**, 10 (1951).
- [29] C.W. Misner and D. H. Sharp, Phys. Rev. **136**, B571 (1964).
- [30] W. A. Hiscock, L. G. Williams and D. M. Eardley, Phys. Rev. D **26** (1982) 751.
- [31] J. A. Kollmeier *et al.*, Astrophys. J. **648** (2006) 128 [arXiv:astro-ph/0508657].
- [32] I. Booth and S. Fairhurst, Phys. Rev. D **75** (2007) 084019 [arXiv:gr-qc/0610032].
- [33] L. Andersson, M. Mars and W. Simon, Phys. Rev. Lett. **95** (2005) 111102 [arXiv:gr-qc/0506013].
- [34] E. Gourgoulhon and J. L. Jaramillo, Phys. Rev. D **74** (2006) 087502 [arXiv:gr-qc/0607050].
- [35] S. A. Hayward, Int. J. Mod. Phys. D **20**, 401 (2011) [arXiv:0906.2528 [gr-qc]].